HHS Public Access

Author manuscript

FEBS J. Author manuscript; available in PMC 2023 March 01.

Published in final edited form as:

FEBS J. 2022 March ; 289(6): 1515–1523. doi:10.1111/febs.16158.

The ups and downs of elevator-type di-/tricarboxylate membrane transporters

David B. Sauer[1,&], **Bing Wang**[2], **Joseph C. Sudar**[1], **Jinmei Song**[1], **Jennifer Marden**[1], **William J. Rice**[2], **Da-Neng Wang**[1,3]

[1]Skirball Institute of Biomolecular Medicine, New York University School of Medicine, New York, NY 10016, USA

[2]Cryo-Electron Microscopy Core, New York University School of Medicine, New York, NY 10016, USA

[3]Department of Cell Biology, New York University School of Medicine, New York, NY 10016, USA

Abstract

The divalent anion sodium symporter (DASS) family contains both sodium-driven anion co-transporters and anion/anion exchangers. The family belongs to a broader Ion Transporter Superfamily (ITS), which comprises 24 families of transporters, including those of AbgT antibiotic efflux transporters. The human proteins in the DASS family play major physiological roles and are drug targets. We recently determined multiple structures of the human sodium-dependent citrate transporter (NaCT) and the succinate/dicarboxylate transporter from *Lactobacillus acidophilus* (LaINDY). Structures of both proteins show high degrees of structural similarity to the previously-determined VcINDY fold. Conservation between these DASS protein structures and those from the AbgT familiy indicates that the VcINDY fold represents the overall protein structure for the entire ITS superfamily. The new structures of NaCT and LaINDY are captured in the inward- or outward-facing conformations, respectively. The domain arrangements in these structures agree with a rigid-body elevator-type transport mechanism for substrate translocation across the membrane. Two separate NaCT structures in complex with a substrate or an inhibitor allowed us to explain the inhibition mechanism and propose a detailed classification scheme for grouping disease-causing mutations in the human protein. Structural understanding of multiple kinetic states of DASS proteins is a first step towards the detailed characterization of their entire transport cycle.

Graphical Abstract

Correspondence: Da-Neng Wang, Skirball Institute of Biomolecular Medicine, New York University School of Medicine, 540 First Avenue, New York, NY 10016, USA, Tel: +12122638634, da-neng.wang@med.nyu.edu.

&:Current address: Centre for Medicines Discovery, Nuffield Department of Medicine, University of Oxford, Oxford, UK

Author contributions

All authors participated in the interpretation of the results and in writing the article.

Conflict of interest

The authors declare no conflict of interest.

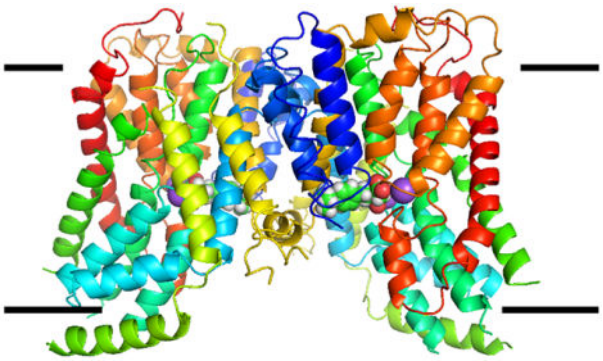

Liver cells import citrate as an energy source and a precursor for fatty acid synthesis. This uptake is accomplished via the Na^+-driven citrate transporter (NaCT) in the plasma membrane. Inhibition of uptake can reduce fat storage. We determined the structure of human NaCT in complex with an inhibitor. The structure reveals how the compound inhibits transport and why it inhibits NaCT selectively over other homologous dicarboxylate transporters in humans.

Keywords

Citrate uptake; membrane transporter structure; SLC13 family; DASS family; ITS superfamily

Introduction

Citrate and various dicarboxylates are TCA cycle intermediates and important energy sources for the cell. Mammalian cells import citrate and dicarboxylates across the plasma membrane via the sodium-dependent citrate transporter (NaCT) and sodium-dependent dicarboxylate transporters 1 and 3 (NaDC1 and NaDC3). These proteins belong to the solute carrier 13 (SLC13) family. SLC13 proteins, together with homologs in bacteria, yeast, plants and flies, are part of the larger ubiquitous divalent anion sodium symporter (DASS) family [1–3]. Although substrate transport of most DASS proteins is sodium-gradient driven, some members of the family from bacteria and plants are exchangers of di- and tricarboxylates, which do not depend on a sodium gradient [4]. Finally, in the broader sense, DASS, along with the other 23 families of transporters for proton, lactate, gluconate, drugs and short-chain fatty acids, together form the Ion Transporter Superfamily (ITS, Pfam: CL0182) [5–7] with 86,180 identified proteins (as of May 21, 2021) (https://pfam.xfam.org/clan/CL0182).

In addition to being TCA cycle intermediates, citrate and dicarboxylates play multiple physiological roles in the cell. Not only is cytosolic citrate a major precursor for fatty acid synthesis, it also activates the first committed enzyme of this synthesis pathway [8] and inhibits a rate-limiting enzyme in glycolysis [9]. Therefore, in liver and adipose cells the cytosolic citrate concentration directly modulates the rate of fatty acid synthesis [10, 11]. In addition to its role in metabolism, citrate also functions as a precursor for the acetyl-CoA synthesis needed for histone acetylation, regulating DNA transcription and replication [12].

In addition to citrate released from mitochondria, cytosolic citrate is imported from the blood across the plasma membrane by the citrate transporter NaCT (SLC13A5) [13–15].

Clinically, elevated NaCT expression is observed in patients with obese, non-alcoholic fatty liver disease. Knocking down NaCT expression significantly decreased the lipid content in hepatic cell lines [16]. *NaCT*-knockout mice have increased hepatic mitochondrial biogenesis and reduced lipogenesis, which taken together protect the mice from obesity and insulin resistance [17]. Finally, in human fetuses and newborns, citrate import via NaCT is particularly crucial for nutrient uptake and brain development [18, 19]. Over fifty mutations in NaCT are found to cause a type of early-onset epileptic encephalopathy named SLC13A5-Epilepsy [20–22].

NaCT's central role in fatty acid biosynthesis makes it a particularly attractive drug target for the treatment of obesity, diabetes and cardiovascular diseases through the reduction of fat storage [17, 23]. Several novel small molecules with a dicarboxylate moiety have been developed as NaCT inhibitors [24, 25]. In particular the compound PF-06649298 (PF2) exhibits both high affinity and specificity for NaCT. The location of the PF2 binding site in NaCT and the nature of the inhibition mechanism, however, are both controversial. Resolving this ambiguity in PF2 binding and inhibition, and explaining its specificity toward NaCT over other human dicarboxylate transporters, requires high-resolution structural information on NaCT.

Extensive functional and biochemical studies have been carried out on both mammalian and bacterial DASS proteins. Available evidence indicates that Na^+-driven DASS cotransporters operate via an ordered sequence, with Na^+ binding preceding substrate binding and Na^+ release following substrate release (Fig. 1) [26–30].

VcINDY structure in its inward-facing conformation

For mechanistic understanding, the first high-resolution structure solved from any member of the DASS family or the ITS superfamily was that of the Na^+-driven dicarboxylate transporter VcINDY from *Vibrio cholerae*, published in 2012 [31]. The structure captured VcINDY in an inward-facing (C_i-Na^+-S) state, with its substrate-binding site open to the cytosol (Fig. 1; Fig. 2). The protein forms a homodimer and each protomer consists of both a scaffold and a transport domain (Fig. 1D). Of the 11 transmembrane helixes in a protomer, TM1–4 and TM7–9 form the scaffold domain, while the transport domain contains TM5, 6, 10, 11, as well as two hairpins, HP_{in} and HP_{out} (Fig. 2A,B). The N-terminal half of the protein TM2–6 and the C-terminal half TM7–11 are related by an inverted pseudo-twofold symmetry. In the transport domain, two carboxylate moieties of the bound substrate are coordinated by two conserved Ser-Asn-Thr (SNT) sequences, which are signature motifs for di-/tricarboxylate DASS transporters and also form part of the Na^+-binding sites Na1 and Na2.

The height of the scaffold domain is insufficient to span the entire lipid bilayer of the membrane, which necessitates the homodimerization of the protein. Structural information, along with cross-linking and computer modeling using an inverted repeat symmetry in the protein sequence [31, 32], suggests that DASS proteins operate through an elevator-type transport mechanism. In this mechanism, the transport domain moves as a rigid body across the membrane, exposing the substrate and sodium binding sites alternatively to the two

sides of the membrane to realize substrate transport. However, the conformational changes associated with DASS family transport remained unknown (Fig. 1B).

LaINDY structure in its outward-facing conformation

As a first step in understanding the conformational changes needed to translocate the substrate between the two sides of the membrane in DASS proteins, we determined the structure of another bacterial member of the transporter family, succinate/dicarboxylate exchanger from *Lactobacillus acidophilus* (LaINDY) (Fig. 1C) [4]. Although a sodium-independent exchanger, LaINDY nevertheless forms a dimer with the same fold as VcINDY. Importantly, the LaINDY structure we captured is in an outward-facing, C_o conformation. The individual domains exhibit strong structural homology to VcINDY, with backbone r.m.s.d.s of 2.8 Å and 2.0 Å for the scaffold and transport domains, respectively. Comparison of domain positions between the LaINDY C_o structure with the VcINDY C_i structure confirms the elevator-type of rigid-body conformational changes needed for substrate translocation in DASS proteins.

Unlike Na^+-dependent cotransporters in the DASS family, the two "Na^+ binding sites" in the DASS exchanger subfamily are each occupied by a conserved, positively-charged residue that acts as Na^+ surrogate [4]. This observation strongly suggests that charge compensation [33, 34] is crucial for reducing the energy barrier in DASS proteins for translocating charged substrates across the hydrophobic lipid bilayer. Like Brownian motion [35], such charge compensation may be important to the transport of charged substrates in other membrane transporters, both co-transporters and exchangers [36].

Conformational changes between outward- and inward-facing states

To further characterize the conformational changes of DASS proteins during substrate translocation, our collaborators Trebesch and Tajkhoshid carried out biased molecular dynamics (MD) simulations on LaINDY [4] (Fig. 1E,F). The simulations revealed a rigid body movement of the transport domain between the C_o-S and C_i-S states through a 39° rotation and an 8.3 Å translation (Fig. 1C), agreeing well with the differences in transport domain position between VcINDY and LaINDY. Two horizontal helixes, H4c and H9c, are rigidly attached to the scaffold domain in order to support this rotation and translation. Such conformational changes are believed to be conserved among DASS family members, including human NaCT.

The VcINDY fold represents the overall structure for the entire Ion Transport Superfamily

The structural conservation between the VcINDY and LaINDY proteins provides strong evidence that the VcINDY fold is representative of the entire DASS family. Based on observations on other membrane transporter superfamilies [37, 38], it follows that other families in the ITS superfamily may adopt the same VcINDY fold [31, 39]. Furthermore, this suggests that members of the ITS superfamily bind substrate at the same location as

seen in VcINDY and use an elevator-type transport mechanism for substrate translocation across the membrane.

In addition to the DASS family, another group of proteins in the ITS superfamily that has been structurally characterized is the AbgT family. The structures of MtrF from *Neisseria gonorrhoeae* and YdaH from *Alcanivorax borkumensis* were reported in 2015 [40, 41]. Both AbgT proteins are believed to function as antimicrobial efflux pumps. Like VcINDY, both MtrF and YdaH exist as homodimers, with the scaffold domains forming the dimer interface (Fig. 2C). Extensive bioinformatics analysis has shown structures of these AbgT proteins are highly similar to that of VcINDY [39]. The backbone α-carbon r.m.s.d.s of MtrF and YdaH versus VcINDY are 4.3 Å and 4.6 Å, respectively. If only the transport domains are considered, the differences drop to 3.3 Å and 2.9 Å respectively. At the equivalent position of the Na2 in VcINDY, a density for sodium is found in the YdaH structure. Such structural conservation between distantly related proteins supports the notion that the VcINDY fold represents the entire ITS superfamily.

While the fold and oligomeric state of VcINDY represent the members of the ITS superfamily, the structural conservation of its transport domain alone actually extends beyond the ITS superfamily. The transport domain of the concentrative nucleotide transporters (CNTs) [42, 43] share high structural similarity with that of VcINDY (Fig. 2D). The *Vibrio cholerae* CNT (VcCNT) and VcINDY proteins have a backbone α-carbon r.m.s.d. of 6.2 Å over their transport domains (HP1, TM4, TM5 from the N-terminal half, and HP2, TM7, TM11 from the C-terminal half in VcCNT; HP_{in}, TM5, TM6, and HP_{out}, TM10, TM11 in VcINDY). However, when the N- and C-terminal halves are compared separately, the r.m.s.d.s drops to 3.8 Å and 6.1 Å, respectively, indicating varied assembly of the N- and C-terminal halves in the transport domains on the two transporters. The substrate translocation in VcCNT is driven by one Na^+, and the Na^+ site is structurally equivalent to the Na1 site in VcINDY. Interestingly, the scaffold domain architecture of VcCNT is completely different, and the protein forms a homotrimer. Three long horizontal helixes, one from each protomer, provide a backbone framework for the movement of the transport domains. Additionally, structural modeling and mutagenesis analysis have shown that the transport domain of the Na^+-dependent phosphate transporter NaPi-II, a member of the SLC34 family, is similar to the transport domain of VcINDY [44, 45].

Finally, it is worth comparing the structures of the bacterial Na^+-driven citrate transporter CitS [46, 47] to that of VcINDY [48]. The two proteins have an insignificant amino acid sequence identity of ~14%. Whereas CitS also forms a dimer, with each protomer consisting of a scaffold and a transport domain, the r.m.s.d. of the backbone α-carbons between CitS and VcINDY is ~20 Å. In contrast to the VcINDY transport domain that consists of two HP-TM-TM motifs (Fig. 2A), in the CitS motifs the hairpin is sandwiched between two transmembrane helices (i.e. TM-HP-TM). As a result, the hairpins insert into the membrane in opposite directions between the two transporters. Interestingly, two hairpins in CitS intersect in the middle of the transporter and form the first Na^+ binding site, with a second Na^+ located toward the cytosol. This arrangement is distinct from VcINDY, where two hairpins each interact with a long loop to form two separate sodium sites at the same depth from the membrane surface.

Human NaCT structure in its inward-facing conformation

We recently determined an inward-facing structure of the human citrate transporter NaCT in complex with citrate and Na^+, the first structure of a mammalian DASS protein (Fig. 3A) [49]. Requiring a specialized tilted cryo-EM data collection strategy [50], the NaCT structure resembles its bacterial homologs (Fig. 1) [4, 31, 51]. The dimer organization, the domain architecture and the transmembrane topology are all similar. In the transport domain, the two SNT signature motifs, the locations of the substrate-binding site and the Na^+ sites Na1 and Na2 are all conserved with VcINDY. Due to weak scattering to electrons by the lithium ions needed for stabilizing the protein for cryo-EM structure determination, the locations of the two remaining Na^+ sites have yet to be identified. Similarly, as the triple-negatively charged citrate is particularly sensitive to electron radiation damage, the quality of the substrate density is insufficient for detailed description on how the protein discriminates various di/-tricarboxylates.

Inhibition mechanism of NaCT by Pfizer compounds

Building on the NaCT-Citrate structure, we also examined the specificity and inhibition mechanism of the Pfizer compounds by determining the structure of NaCT in the presence of sodium and Pfizer compound PF2 (Fig. 3) [49]. Notably, within the NaCT-PF2 complex structure was an additional density, easily identified as the inhibitor.

The PF2 compound binds at the same location on the cytosolic side of the protein as the substrate in our NaCT-citrate structure (Fig. 3B). Such overlapping binding sites supports the previously proposed mechanism of competitive inhibition [24, 25, 52]. Interactions of PF2 with the cytosolic surface of the scaffold domain block the sliding movement of the transport domain towards the extracellular direction (Fig. 3C). Simultaneously, PF2 binding with the transport domain prevents sodium release and stops the C_i-Na^+-S to C_i-Na^+ state transition (Figs. 1A,B). Unable to undergo structural or chemical transitions, NaCT bound to PF2 is thus inhibited from citrate transport.

PF2 is highly specific for human NaCT, with significantly weaker inhibition of the homologous dicarboxylate transporters, NaDC1 and NaDC3 [24, 25, 52]. The NaCT structures reveal this selectivity is caused by the presence of Gly409 in NaCT's scaffold domain, which directly interacts with the isobutyl group of PF2 (Fig. 3D). In contrast, asparagine is found at the equivalent position in both NaDC3 and NaDC1. This larger side chain would sterically clash with PF2, reducing its binding and inhibition to the two dicarboxylate transporters. Finally, we observed that the large inhibitor binding pocket can be utilized to increase the affinity of the inhibitor and its selectivity towards NaCT.

NaCT structure allowed detailed classification of SLC13A5-Epilepsy mutations

The locations of the SLC13A5-Epilepsy mutations within the NaCT structure allowed us to explain how each abolish NaCT's transport activity [20–22]. Previously, cellular localization and biochemical analyses of clinical loss-of-function mutants [18, 19] had suggested two

types of pathogenesis [22]: Type I mutations affect the localization and stability of the protein, while Type II directly abolishes transport activity. Now we can further classify each type based on their location in the three-dimensional structure of the protein. Among the Type I mutations, Type Ia are nonsense or frame shift mutations that result in incomplete protein molecules, while Type Ib mutations are hypothesized to destabilize the transporter. Within the fully expressed but inactive Type II mutants, Type IIa are close to the citrate and Na^+ binding sites and are therefore expected to alter substrate or cation binding. Finally, mutations located at the interface between the scaffold and transport domains (Type IIb) likely obstruct the movement of the transport domain during substrate translocation. This better understanding of each type of mutation suggests that separate therapeutic strategies will be most effective in treating SLC13A5-Epilepsy.

Unanswered mechanistic questions

The VcINDY structure represents not only that of the DASS family, but also represents a general fold found across the entire ITS superfamily of membrane transporters. Structural determination of DASS proteins in both inward- and outward-facing conformations represent significant advances in the mechanistic understanding of this family of transporters. The human NaCT structures provide a solid foundation for understanding the mechanism of inhibition and molecular pathogenesis of SLC13A5-Epilepsy. These recent structures pose new questions for the field: Where are the two additional bound sodium ions in NaCT? And what is the structural basis for substrate – sodium coupling in DASS proteins [53]? How does the transporter convert between the outward-facing and inward-facing states? Perhaps, structural biology and biochemical techniques, along with molecular dynamics simulations and experimental techniques for studying protein dynamics such as single molecular fluorescence spectroscopy, electron paramagnetic resonance and atomic force microscopy [54], will allow us to better understand the entire transport cycle of DASS proteins. Instead of looking at snapshots, we will be watching molecular movies.

Acknowledgements

This work was financially supported by the NIH (R01NS108151, R01GM121994, and R01DK099023), the G. Harold and Leila Y. Mathers Foundation, the TESS Research Foundation, the American Epilepsy Society and Pfizer Inc. D.B.S. was supported by the American Cancer Society Postdoctoral Fellowship (129844-PF-17-135-01-TBE) and Department of Defense Horizon Award (W81XWH-16-1-0153). We are grateful to our collaborators for their contributions to the work reviewed here: J.K. Hilton, A. Koide, S. Koide, J.A. Mindell, E. Tajkhorshid and N. Trebesch. We also thank the current and former group members for contributions and discussions: N. Cocco, G.G. Gregorio, N.K. Karpowich, R. Mancusso, F. Ono and A.B. Rejto. We thank the staff at the following facilities for data collection: the Simons Electron Microscopy Center at the New York Structural Biology Center, National Center for CryoEM Access and Training and the Pacific Northwest Center for Cryo-EM.

Data Accessibility Statement

The unaligned electron micrographs used for the NaCT-citrate structure have been deposited in EMPIAR (ID: EMPIAR-10728).

Abbreviations

AbgT	the *p*-aminobenzoyl-glutamate transporter family

CitS	bacterial sodium-citrate symporter
CNT	concentrative nucleotide transporter
cryo-EM	cryo-electron microscopy
DASS	divalent anion sodium symporter
HP	hairpin helix
ITS	Ion Transporter Superfamily
LAINDY	succinate/dicarboxylate exchanger from *Lactobacillus acidophilus*
MtrF	antimicrobial efflux protein from *Alcanivorax borkumensis*
NaCT	mammalian sodium-dependent citrate transporter
NaDC1	mammalian sodium-dependent dicarboxylate transporter 1
NaDC3	mammalian sodium-dependent dicarboxylate transporter 3
PF2	Pfizer compound PF-06649298
r.m.s.d.	root-mean-square deviation
SLC13	solute carrier family 13
TCA cycle	tricarboxylic acid cycle
TM	transmembrane α-helix
VcCNT	concentrative nucleotide transporter from *Vibrio cholerae*
VcINDY	sodium-dependent dicarboxylate transporter from *Vibrio cholerae*
YdaH	antimicrobial efflux protein from *Alcanivorax borkumensis*

References

[1]. Markovich D, Murer H. The SLC13 gene family of sodium sulphate/carboxylate cotransporters. Pflug Arch Eur J Phy. 2004;447:594–602.

[2]. Bergeron MJ, Clemencon B, Hediger MA, Markovich D. SLC13 family of Na^+-coupled di- and tri-carboxylate/sulfate transporters. Mol Aspects Med. 2013;34:299–312. [PubMed: 23506872]

[3]. Pajor AM. Sodium-coupled dicarboxylate and citrate transporters from the SLC13 family. Pflugers Arch. 2014;466:119–30. [PubMed: 24114175]

[4]. Sauer DB, Trebesch N, Marden JJ, Cocco N, Song J, Koide A, et al. Structural basis for the reaction cycle of DASS dicarboxylate transporters. eLife. 2020;9.

[5]. Prakash S, Cooper G, Singhi S, Saier MH. The ion transporter superfamily. Bba-Biomembranes. 2003;1618:79–92. [PubMed: 14643936]

[6]. Lolkema JS, Slotboom DJ. Classification of 29 families of secondary transport proteins into a single structural class using hydropathy profile analysis. J Mol Biol. 2003;327:901–9. [PubMed: 12662917]

[7]. Chen JS, Reddy V, Chen JH, Shlykov MA, Zheng WH, Cho J, et al. Phylogenetic characterization of transport protein superfamilies: superiority of SuperfamilyTree programs over those based on multiple alignments. J Mol Microbiol Biotechnol. 2011;21:83–96. [PubMed: 22286036]

[8]. Spencer AF, Lowenstein JM. Supply of precursors for synthesis of fatty acids. J Biol Chem. 1962;237:3640–8. [PubMed: 13990010]

[9]. Sul HS, Smith S. Fatty acid synthesis in eukaryotes. In: Vance DE, Vance JE, editors. Biochemistry of Lipids, Lipoproteins and Membranes. 5th ed. New York: Elsevier; 2008. p. 155–90.

[10]. Fang M, Lowenstein JM. Citrate and the conversion of carbohydrate into fat. The regulation of fatty acid synthesis by rat liver extracts. Biochem J. 1967;105:803–11. [PubMed: 5584019]

[11]. Shrago E, Spennetta T, Gordon E. Fatty acid synthesis in human adipose tissue. J Biol Chem. 1969;244:2761–6. [PubMed: 5770000]

[12]. Wellen KE, Hatzivassiliou G, Sachdeva UM, Bui TV, Cross JR, Thompson CB. ATP-citrate lyase links cellular metabolism to histone acetylation. Science. 2009;324:1076–80. [PubMed: 19461003]

[13]. Inoue K, Zhuang L, Maddox DM, Smith SB, Ganapathy V. Structure, function, and expression pattern of a novel sodium-coupled citrate transporter (NaCT) cloned from mammalian brain. J Biol Chem. 2002;277:39469–76. [PubMed: 12177002]

[14]. Inoue K, Fei YJ, Zhuang LN, Gopal E, Miyauchi S, Ganapathy V. Functional features and genomic organization of mouse NaCT, a sodium-coupled transporter for tricarboxylic acid cycle intermediates. Biochem J. 2004;378:949–57. [PubMed: 14656221]

[15]. Gopal E, Miyauchi S, Martin PM, Ananth S, Srinivas SR, Smith SB, et al. Expression and functional features of NaCT, a sodium-coupled citrate transporter, in human and rat livers and cell lines. Am J Physiol-Gastr L. 2007;292:G402–G8.

[16]. Li L, Li H, Garzel B, Yang H, Sueyoshi T, Li Q, et al. SLC13A5 is a novel transcriptional target of the pregnane X receptor and sensitizes drug-induced steatosis in human liver. Molecular pharmacology. 2015;87:674–82. [PubMed: 25628225]

[17]. Birkenfeld AL, Lee HY, Guebre-Egziabher F, Alves TC, Jurczak MJ, Jornayvaz FR, et al. Deletion of the mammalian INDY homolog mimics aspects of dietary restriction and protects against adiposity and insulin resistance in mice. Cell Metab. 2011;14:184–95. [PubMed: 21803289]

[18]. Yang QZ, Spelbrink EM, Nye KL, Hsu ER, Porter BE. Epilepsy and EEG Phenotype of SLC13A5 Citrate Transporter Disorder. Child Neurol Open. 2020;7:2329048X20931361.

[19]. Matricardi S, De Liso P, Freri E, Costa P, Castellotti B, Magri S, et al. Neonatal developmental and epileptic encephalopathy due to autosomal recessive variants in SLC13A5 gene. Epilepsia. 2020;61:2474–85. [PubMed: 33063863]

[20]. Thevenon J, Milh M, Feillet F, St-Onge J, Duffourd Y, Juge C, et al. Mutations in SLC13A5 cause autosomal-recessive epileptic encephalopathy with seizure onset in the first days of life. Am J Hum Genet. 2014;95:113–20. [PubMed: 24995870]

[21]. Hardies K, de Kovel CG, Weckhuysen S, Asselbergh B, Geuens T, Deconinck T, et al. Recessive mutations in SLC13A5 result in a loss of citrate transport and cause neonatal epilepsy, developmental delay and teeth hypoplasia. Brain. 2015;138:3238–50. [PubMed: 26384929]

[22]. Klotz J, Porter BE, Colas C, Schlessinger A, Pajor AM. Mutations in the Na^+/citrate cotransporter NaCT (SLC13A5) in pediatric patients with epilepsy and developmental delay. Mol Med. 2016;22:310–21. [PubMed: 27261973]

[23]. Willmes DM, Kurzbach A, Henke C, Schumann T, Zahn G, Heifetz A, et al. The longevity gene INDY (I'm Not Dead Yet) in metabolic control: Potential as pharmacological target. Pharmacol Ther. 2018;185:1–11. [PubMed: 28987323]

[24]. Huard K, Brown J, Jones JC, Cabral S, Futatsugi K, Gorgoglione M, et al. Discovery and characterization of novel inhibitors of the sodium-coupled citrate transporter (NaCT or SLC13A5). Sci Rep. 2015;5:17391. [PubMed: 26620127]

[25]. Huard K, Gosset JR, Montgomery JI, Gilbert A, Hayward MM, Magee TV, et al. Optimization of a dicarboxylic series for *in Vivo* inhibition of citrate transport by the solute carrier 13 (SLC13) family. J Med Chem. 2016;59:1165–75. [PubMed: 26734723]

[26]. Wright SH, Hirayama B, Kaunitz JD, Kippen I, Wright EM. Kinetics of sodium succinate cotransport across renal brush-border membranes. J Biol Chem. 1983;258:5456–62. [PubMed: 6853527]

[27]. Yao X, Pajor AM. The transport properties of the human renal Na^+-dicarboxylate cotransporter under voltage-clamp conditions. Am J Physiol Renal Physiol. 2000;279:F54–64. [PubMed: 10894787]

[28]. Hall JA, Pajor AM. Functional characterization of a Na^+-coupled dicarboxylate carrier protein from *Staphylococcus aureus*. J Bacteriol. 2005;187:5189–94. [PubMed: 16030212]

[29]. Pajor AM, Sun NN, Leung A. Functional characterization of SdcF from *Bacillus licheniformis*, a homolog of the SLC13 Na^+/dicarboxylate transporters. J Membr Biol. 2013;246:705–15. [PubMed: 23979173]

[30]. Mulligan C, Fitzgerald GA, Wang DN, Mindell JA. Functional characterization of a Na^+-dependent dicarboxylate transporter from *Vibrio cholerae*. J Gen Physiol. 2014;143:745–59. [PubMed: 24821967]

[31]. Mancusso R, Gregorio GG, Liu Q, Wang DN. Structure and mechanism of a bacterial sodium-dependent dicarboxylate transporter. Nature. 2012;491:622–6. [PubMed: 23086149]

[32]. Mulligan C, Fenollar-Ferrer C, Fitzgerald GA, Vergara-Jaque A, Kaufmann D, Li Y, et al. The bacterial dicarboxylate transporter VcINDY uses a two-domain elevator-type mechanism. Nature structural & molecular biology. 2016;23:256–63.

[33]. Grewer C, Zhang Z, Mwaura J, Albers T, Schwartz A, Gameiro A. Charge compensation mechanism of a Na^+-coupled, secondary active glutamate transporter. J Biol Chem. 2012;287:26921–31. [PubMed: 22707712]

[34]. Nath S Charge transfer across biomembranes: A solution to the conundrum of high desolvation free energy penalty in ion transport. Biophys Chem. 2021;275:106604. [PubMed: 33957504]

[35]. Law CJ, Yang Q, Soudant C, Maloney PC, Wang DN. Kinetic evidence is consistent with the rocker-switch mechanism of membrane transport by GlpT. Biochemistry. 2007;46:12190–7. [PubMed: 17915951]

[36]. Law CJ, Enkavi G, Wang DN, Tajkhorshid E. Structural basis of substrate selectivity in the glycerol-3-phosphate:phosphate antiporter. Biophys J. 2009;97:1346–53. [PubMed: 19720022]

[37]. Law CJ, Maloney PC, Wang DN. Ins and outs of major facilitator superfamily antiporters. Annu Rev Microbiol. 2008;62:289–305. [PubMed: 18537473]

[38]. Forrest LR, Rudnick G. The rocking bundle: a mechanism for ion-coupled solute flux by symmetrical transporters. Physiology (Bethesda, Md. 2009;24:377–86. [PubMed: 19996368]

[39]. Vergara-Jaque A, Fenollar-Ferrer C, Mulligan C, Mindell JA, Forrest LR. Family resemblances: A common fold for some dimeric ion-coupled secondary transporters. J Gen Physiol. 2015;146:423–34. [PubMed: 26503722]

[40]. Su C-C, Bolla JR, Kumar N, Radhakrishnan A, Long F, Delmar JA, et al. Structure and function of Neisseria gonorrhoeae MtrF illuminates a class of antimetabolite efflux pumps. Cell reports. 2015;11:61–70. [PubMed: 25818299]

[41]. Bolla JR, Su C-C, Delmar JA, Radhakrishnan A, Kumar N, Chou T-H, et al. Crystal structure of the *Alcanivorax borkumensis* YdaH transporter reveals an unusual topology. Nature communications. 2015;6:6874.

[42]. Johnson ZL, Cheong CG, Lee SY. Crystal structure of a concentrative nucleoside transporter from *Vibrio cholerae* at 2.4 Å. Nature. 2012;483:489–93. [PubMed: 22407322]

[43]. Johnson ZL, Lee JH, Lee K, Lee M, Kwon DY, Hong J, et al. Structural basis of nucleoside and nucleoside drug selectivity by concentrative nucleoside transporters. eLife. 2014;3:e03604. [PubMed: 25082345]

[44]. Fenollar-Ferrer C, Patti M, Knopfel T, Werner A, Forster IC, Forrest LR. Structural fold and binding sites of the human Na^+-phosphate cotransporter NaPi-II. Biophys J. 2014;106:1268–79. [PubMed: 24655502]

[45]. Fenollar-Ferrer C, Forrest LR. Structural models of the NaPi-II sodium-phosphate cotransporters. Pflugers Arch. 2019;471:43–52. [PubMed: 30175376]

[46]. Wohlert D, Grotzinger MJ, Kühlbrandt W, Yildiz O. Mechanism of Na^+-dependent citrate transport from the structure of an asymmetrical CitS dimer. eLife. 2015;4:e09375. [PubMed: 26636752]

[47]. Kim JW, Kim S, Kim S, Lee H, Lee J-O, Jin MS. Structural insights into the elevator-like mechanism of the sodium/citrate symporter CitS. Scientific reports. 2017;7:2548. [PubMed: 28566738]

[48]. Lolkema JS, Slotboom DJ. Structure and elevator mechanism of the Na^+-citrate transporter CitS. Current opinion in structural biology. 2017;45:1–9. [PubMed: 27776291]

[49]. Sauer DB, Song J, Wang B, Hilton JK, Karpowich NK, Mindell JA, et al. Structure and inhibition mechanism of the human citrate transporter NaCT. Nature 2021;591:157–61. [PubMed: 33597751]

[50]. Tan YZ, Baldwin PR, Davis JH, Williamson JR, Potter CS, Carragher B, et al. Addressing preferred specimen orientation in single-particle cryo-EM through tilting. Nat Methods. 2017;14:793–6. [PubMed: 28671674]

[51]. Nie R, Stark S, Symersky J, Kaplan RS, Lu M. Structure and function of the divalent anion/Na^+ symporter from *Vibrio cholerae* and a humanized variant. Nat Commun. 2017;8:15009. [PubMed: 28436435]

[52]. Pajor AM, de Oliveira CA, Song KC, Huard K, Shanmugasundaram V, Erion DM. Molecular basis for inhibition of the Na^+/citrate transporter NaCT (SLC13A5) by dicarboxylate Inhibitors. Molecular pharmacology. 2016;90:755–65. [PubMed: 27683012]

[53]. Sampson CDD, Stewart MJ, Mindell JA, Mulligan C. Solvent accessibility changes in a Na^+-dependent C4-dicarboxylate transporter suggest differential substrate effects in a multistep mechanism. J Biol Chem. 2020;295:18524–38. [PubMed: 33087444]

[54]. Karpowich NK, Wang DN. Biophysics: Transporter in the spotlight. Nature. 2010;465:171–2. [PubMed: 20463728]

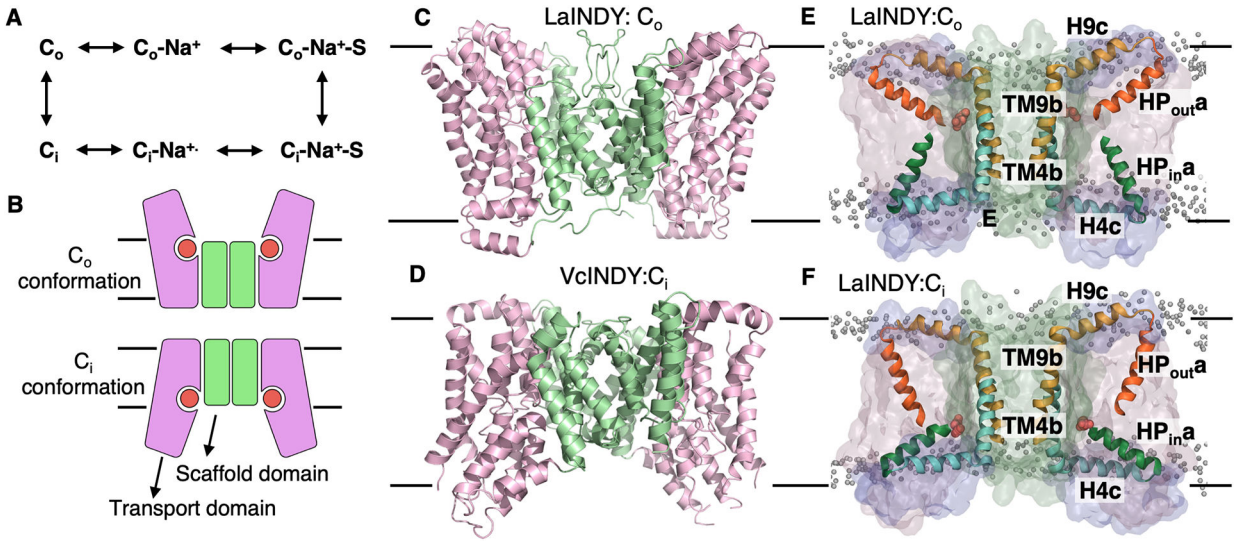

Fig. 1.

Kinetic cycle and outward- and inward-facing conformations of DASS proteins. A. Kinetic cycle of Na+-dependent DASS co-transporters. C_o: outward-facing state. C_i: inward-facing state. S: substrate. B. Schematic drawing showing the outward- and inward-facing conformations of DASS proteins. The proteins form homodimers, with each protomer comprising a scaffold domain (green) and a transport domain (pink). For substrate translocation across the membrane, the transport domain undergoes elevator-type movements, exposing the substrate binding site alternatively to the extracellular space and the cytosol. C. Outward-facing structure of LaINDY [4]. Although the protein is a succinate/dicarboxylate exchanger, independent of the Na^+-gradient, its structure is homologous to the Na^+-dependent dicarboxylate transporter VcINDY. D. Inward-facing structure of Na^+-dependent dicarboxylate transporter from *Vibrio cholerae* VcINDY [4]. E. Representative MD structure from the simulation of the LaINDY C_o-S state. F. Representative MD structure from the simulation of the LaINDY C_i-S state. Transition between the C_o-S state to the C_i-S state in LaINDY has been visualized in MD simulations [4]. The scaffold and transport domains in C – F are colored similarly as in B. Figure reproduced from [4], and the figure was generated using PyMol and VMD.

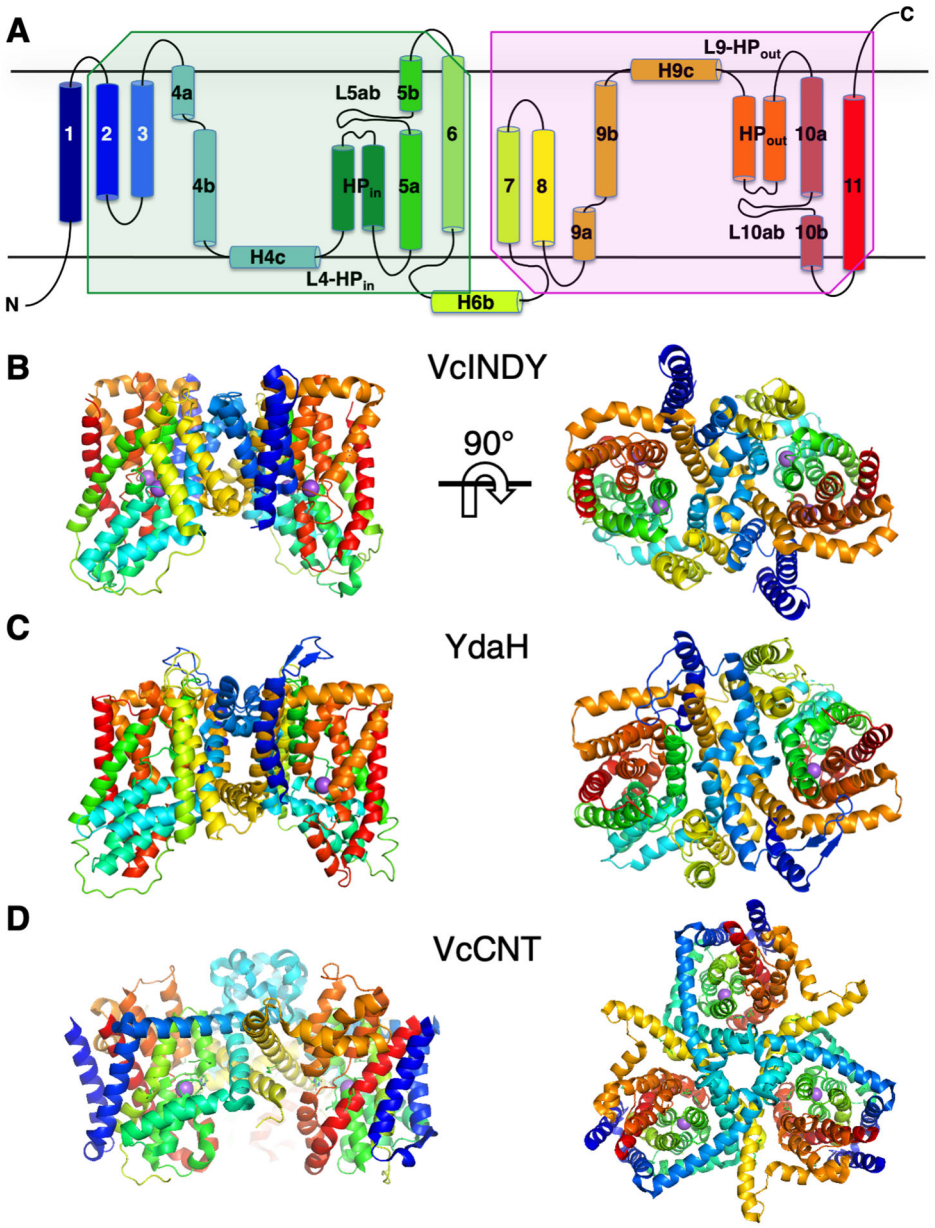

Fig. 2.

Structure conservation of the ITS superfamily and the VcINDY fold. A. Transmembrane topology of VcINDY. The N-terminal half (except TM1) is related to the C-terminal half by an inverted repeat symmetry. Each half contains a hairpin helix and a broken helix with a long loop in the middle. The tip of the hairpin helix and the long loop form a sodium binding site. The substrate binding site is located between these two sodium sites [31]. B. Inward-facing structure of VcINDY, viewed from the membrane plane (left) and from the extracellular space (right) [4, 31, 51]. The protein is a member of the DASS family. C. Structure of antimicrobial efflux protein YdaH [41]. This protein, along with the MtrF protein, are members of the AbgT family. DASS and AbgT families all belong to the Ion Transporter Superfamily. It is proposed that all members of the ITS superfamily adopts

the VcINDY fold. D. Structure of the bacterial concentrative nucleotide transporter VcCNT [42, 43]. Although not a member of the ITS superfamily, the transport domain of VcCNT is similar to that of VcINDY. All structures shown in B – D are in their inward-facing conformation, and the helices are colored by the rainbow scheme. Panels A and B of the figure reproduced from [31], and the figure was generated using PyMol.

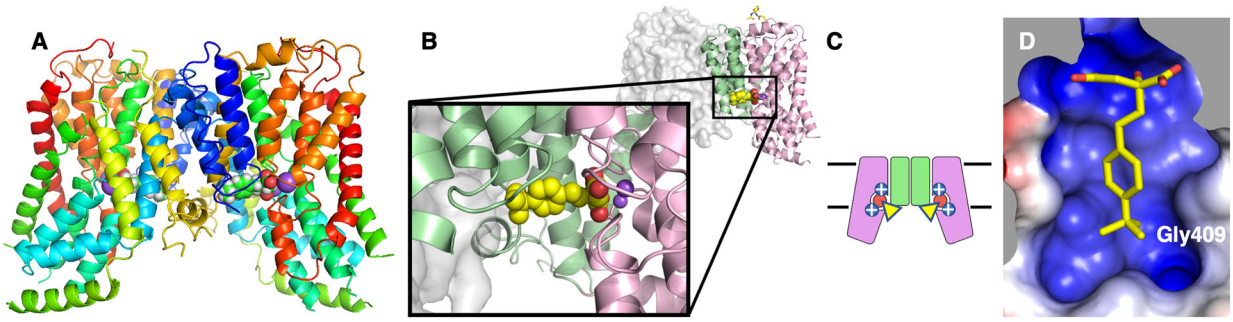

Fig. 3.

Structural basis of the inhibition mechanism and selectivity of PF2 in NaCT [49]. A. Cryo-EM structure of the NaCT-PF2 complex, viewed from within the membrane plane. This structure is highly homologous to that of the protein bound to the citrate substrate. B. PF2 binding site viewed from within the membrane. The dicarboxylate moiety of PF2 binds at the citrate site in the transport domain (pink), whereas PF2's benzene ring and isobutyl group interact with the scaffold domain (green) of NaCT. C. Schematic drawing showing the proposed inhibition mechanism of NaCT by PF2. In each protomer, the dicarboxylate moiety of PF2 (red circle) binds to the citrate site of NaCT in its inward-facing, C_i-Na^+-S state, and blocks sodium release from the Na1 and Na2 sites. At the same time, the modified benzene ring of PF2 (yellow triangle) interacts with the scaffold domain, preventing the transition of the transport domain to an outward-facing conformation. Together, the two types of interactions arrest the transporter in its C_i-Na^+-S state and inhibit transport. D. PF2 binding site shown as electrostatic surface, colored by electrostatic potential of the protein atomic model. Figure and accompanying legend reproduced from [49], and the figure was generated using PyMol.